

RESEARCH

Open Access



Cortico-basal ganglia white matter microstructure is linked to restricted repetitive behavior in autism spectrum disorder

Bradley J. Wilkes^{1*}, Derek B. Archer^{2,3}, Anna L. Farmer⁴, Carly Bass⁵, Hannah Korah⁶, David E. Vaillancourt^{1,7,8} and Mark H. Lewis^{4,5}

Abstract

Background Restricted repetitive behavior (RRB) is one of two behavioral domains required for the diagnosis of autism spectrum disorder (ASD). Neuroimaging is widely used to study brain alterations associated with ASD and the domain of social and communication deficits, but there has been less work regarding brain alterations linked to RRB.

Methods We utilized neuroimaging data from the National Institute of Mental Health Data Archive to assess basal ganglia and cerebellum structure in a cohort of children and adolescents with ASD compared to typically developing (TD) controls. We evaluated regional gray matter volumes from T1-weighted anatomical scans and assessed diffusion-weighted scans to quantify white matter microstructure with free-water imaging. We also investigated the interaction of biological sex and ASD diagnosis on these measures, and their correlation with clinical scales of RRB.

Results Individuals with ASD had significantly lower free-water corrected fractional anisotropy (FA_T) and higher free-water (FW) in cortico-basal ganglia white matter tracts. These microstructural differences did not interact with biological sex. Moreover, both FA_T and FW in basal ganglia white matter tracts significantly correlated with measures of RRB. In contrast, we found no significant difference in basal ganglia or cerebellar gray matter volumes.

Limitations The basal ganglia and cerebellar regions in this study were selected due to their hypothesized relevance to RRB. Differences between ASD and TD individuals that may occur outside the basal ganglia and cerebellum, and their potential relationship to RRB, were not evaluated.

Conclusions These new findings demonstrate that cortico-basal ganglia white matter microstructure is altered in ASD and linked to RRB. FW in cortico-basal ganglia and intra-basal ganglia white matter was more sensitive to group differences in ASD, whereas cortico-basal ganglia FA_T was more closely linked to RRB. In contrast, basal ganglia and cerebellar volumes did not differ in ASD. There was no interaction between ASD diagnosis and sex-related differences in brain structure. Future diffusion imaging investigations in ASD may benefit from free-water estimation and correction in order to better understand how white matter is affected in ASD, and how such measures are linked to RRB.

Keywords Autism spectrum disorder, Restricted repetitive behavior, Diffusion tensor imaging, Free-water, Basal ganglia, Cerebellum, Cortico-basal ganglia, Gray matter, White matter

*Correspondence:

Bradley J. Wilkes
bwilkes@ufl.edu

Full list of author information is available at the end of the article



This is a U.S. Government work and not under copyright protection in the US; foreign copyright protection may apply 2024. **Open Access** This article is licensed under a Creative Commons Attribution 4.0 International License, which permits use, sharing, adaptation, distribution and reproduction in any medium or format, as long as you give appropriate credit to the original author(s) and the source, provide a link to the Creative Commons licence, and indicate if changes were made. The images or other third party material in this article are included in the article's Creative Commons licence, unless indicated otherwise in a credit line to the material. If material is not included in the article's Creative Commons licence and your intended use is not permitted by statutory regulation or exceeds the permitted use, you will need to obtain permission directly from the copyright holder. To view a copy of this licence, visit <http://creativecommons.org/licenses/by/4.0/>. The Creative Commons Public Domain Dedication waiver (<http://creativecommons.org/publicdomain/zero/1.0/>) applies to the data made available in this article, unless otherwise stated in a credit line to the data.

Background

Autism spectrum disorder (ASD) includes two diagnostic domains: (1) social and communication deficits and (2) restricted repetitive behavior (RRB). RRB refers to multiple categories of repeating patterns of behavior that often occur with high frequency, have no clear function, interfere with appropriate behavior, and can sometimes result in bodily harm. Although many research and intervention efforts in ASD have targeted social and communication deficits, there has been considerably less focus on the RRB domain. Although behavioral interventions have some efficacy in treating RRB [1–3], pharmacological interventions have no demonstrated efficacy for treating RRB in ASD, but rather are used primarily to treat associated problems (e.g., aggressive behavior) [4, 5]. This lack of efficacious treatments is largely due to an incomplete understanding of the neural circuitry mediating RRB in ASD. There is a pressing need to elucidate how RRB relates to differences in brain structure and function in ASD.

There has been increasing focus on hypotheses regarding brain connectivity in ASD, and how disrupted connectivity patterns relate to the two diagnostic domains. Investigations of connectivity differences in ASD have largely utilized magnetic resonance imaging (MRI) to assess structural and functional connectivity. Functional MRI and diffusion tensor imaging (DTI) in ASD both generally support reduced connectivity within major brain networks, though there is also evidence of increased connectivity between networks [6–10]. Although connectivity differences in ASD have frequently been studied in the context of social and communication deficits [11], far fewer studies have focused on altered connectivity as it pertains to RRB. [12]

Scalar measures from DTI provide insight into tissue microstructure and can be used to characterize structural aspects of brain connectivity. These scalar measures are confounded by partial volume effects from free-water (FW), such as cerebrospinal fluid. Using a two-compartment model, the unique contribution of FW can be quantified and other scalar measures adjusted accordingly [13]. The FW measure itself has already demonstrated significant value in a variety of neurodegenerative disorders and it is hypothesized that abnormal FW values are associated with atrophy and/or inflammation [14–19]. Despite the widespread use of DTI to study connectivity in ASD, FW quantification and correction have had limited application in this population [20, 21]. Many of the brain regions and white matter tracts hypothesized to be involved in the expression of RRB in ASD are proximal to the ventricular system, and as such, FW quantification may be of great value to DTI research in ASD.

In this study, we assessed gray matter volume and white matter microstructure in the basal ganglia and cerebellum in individuals with ASD compared to typically developing (TD) participants. We focused on the basal ganglia and cerebellum because they have been linked to RRB and ASD in prior work, yet these relationships remain poorly understood [12, 22–24]. We further investigated whether these measures differed between males and females with ASD, and whether they correlated with clinical measures of RRB. Current estimates suggest ASD is approximately four times more prevalent in males than females [25], and some imaging studies have suggested that the sex differences in brain morphology and connectivity in ASD are unlike those observed in TD individuals [26–31]. There is also mixed evidence of sex differences in the expression of RRB in ASD [32–36]. It remains unknown whether possible sex differences in the expression of RRB relate to sex differences in brain morphology or microstructure. In the present study, we used clinical and neuroimaging data available from the [National Institute of Mental Health Data Archive](#) (NDA) to investigate interactions between ASD diagnosis and biological sex on regional gray matter volumes in the basal ganglia and cerebellum, as well as microstructure in white matter pathways of the basal ganglia and cerebellum. We further investigated the relationship of these neuroimaging measures to clinical measures of RRB.

Methods

Participant data

Deidentified data were acquired from NDA (collection ID #2021). Several key features of this dataset guided our selection including the availability of Repetitive Behavior Scale-Revised scores on participants from both groups, adequate sample sizes, and a nearly equal number of males and females. For our purposes, selection criteria within this dataset included ages between 6 and 18 years, presence of T1-weighted anatomical and diffusion-weighted imaging data, and an intelligence quotient (IQ) measured with the Differential Ability Scales-II. We did not exclude individuals from this study based on IQ score. These data, however, were acquired retrospectively from the NDA and thus we did not have control over recruitment of participants with lower IQ scores. For the ASD group, inclusion also required diagnostic assessments: the Autism Diagnostic Observation Schedule-Second Edition (ADOS-2) and Autism Diagnostic Interview-Revised (ADI-R). Inclusion in the ASD group required an ADOS-2 score of 7 or higher. From the NDA dataset queried, 5 participants originally queried in the ASD dataset (4 males, 1 female) did not meet this cutoff and were excluded from subsequent analysis. Diagnostic assessments were not given to TD participants and thus

were not required for inclusion in the TD group. Application of these initial criteria resulted in a dataset that included 91 individuals diagnosed with ASD (49 female) and 96 TD individuals (44 female). Details about the participants who met these criteria are included in Table 1.

Participants whose data met these initial inclusion criteria were then checked for quality of imaging data (e.g., no missing volumes or major motion artifacts). For anatomical scans, all remaining participants had adequate image quality and no major artifacts and thus were included in volumetric analysis. For diffusion-weighted images, we flagged diffusion volumes (i.e., directions) with more than 2 mm motion. A participant was excluded if more than 25% of their diffusion volumes exceeded this threshold. Applying these criteria, 15 participant’s data were excluded from diffusion MRI analysis (12 ASD, 3 TD).

Magnetic resonance imaging parameters

Images from the broader collection ID (#2021) that these data were acquired from were collected across four sites: (1) The Center for Translational Developmental Neuroscience, Child Study Center, Yale School of Medicine, New Haven, CT; (2) The Nelson Laboratory of Cognitive Neuroscience, Boston Children’s Hospital, Harvard Medical School, Boston, MA; (3) The Center on Human Development & Disability, Seattle Children’s Hospital, University of Washington School of Medicine, Seattle, WA; (4) Staglin IMHRO Center for Cognitive Neuroscience, David Geffen School of Medicine, University of California, Los Angeles, CA. Scans were acquired on 3T Siemens scanners (TrioTim or Prisma) [28, 29]. The study dataset did not contain specific information about the collection site for each participant, but did contain details on the scanner type that each participant was scanned on. Thus, we covaried each imaging analyses by scanner type to control for this source of variability.

Anatomical images were acquired using a T1-weighted magnetization-prepared rapid acquisition gradient-echo (MPRAGE) sequence with the following parameters: 256 single-shot interleaved sagittal slices of 1 mm thickness; field of view (FOV) of 256 mm; 256×256 matrix; repetition time (TR) of 2530 ms; echo time (TE) of 3.31 ms (TrioTim scanners) or 3.34 ms (Prisma scanners), inversion time of 1100 ms; flip angle of 7°; bandwidth of 200 Hz/pixel; 100% phase and slice resolution.

Diffusion-weighted images were acquired using an echo-planar imaging sequence with the following parameters: 60 interleaved transverse slices of 2 mm thickness; 96×96 matrix; FOV of 190 mm; 96×96 matrix; TR of 9000 ms (TrioTim scanners) or 7300 ms (Prisma scanners), TE of 93 ms (TrioTim scanners) or 74 ms (Prisma scanners); echo spacing (δ) of 0.69 ms; 90° flip angle; bandwidth of 2264 Hz/pixel (TrioTim scanners) or 1680 Hz/pixel (Prisma scanners); 100% phase resolution. A diffusion weighting scheme with 64 diffusion directions at $b=1000$ s/mm² and one $b=0$ s/mm² volume was used.

Data analysis

Demographic data and clinical scales

Participant age (in months) and IQ scores were compared using 2×2 analysis of variance (ANOVA) with diagnosis and sex as factors. Analysis of covariance (ANCOVA) was used to investigate effects of diagnosis and sex on repetitive behavior scores from the Repetitive Behavior Scale-Revised (RBS-R) [37], covarying for age. For the RBS-R, we assessed total score, as well as the following six subscale scores: stereotyped behavior, self-injurious behavior, compulsive behavior, ritualistic behavior, sameness behavior, and restricted interests. We also used ANCOVA to investigate effects of diagnosis and sex on social and communication scores from the

Table 1 Demographic data and clinical scales

Group	N	Age in months (StDev)	IQ (StDev)	RBS-R Total (StDev)	ADI-R Section C (StDev)	SCQ (StDev)
<i>ASD</i>						
Male	42	146 (35.4)	102 (18.2)	23.0 (16.1)	6.46 (2.63)	20.4 (6.58)
Female	49	158 (31.9)	102 (22.3)	19.8 (17.4)	5.71 (2.55)	16.4 (7.57)
Total	91	152 (33.9)	102 (20.4)	21.3 (16.8)	6.03 (2.59)	18.3 (7.36)
<i>TD</i>						
Male	52	161 (32.5)	111 (16.2)	2.24 (6.61)	–	3.00 (3.69)
Female	44	157 (38.1)	109 (14.5)	0.98 (1.77)	–	1.77 (2.37)
Total	96	159 (35.0)	110 (15.4)	1.67 (5.07)	–	2.44 (3.20)

Number of participants in each group (ASD or TD) and subgroups of males and females, including means (± StDev) for age, IQ, RBS-R total score, ADI-R section C score, and SCQ score

lifetime version of the Social Communication Questionnaire (SCQ) [38], covarying for age.

For the ADI-R, scores were only available for individuals in the ASD group. Because the primary focus of this paper was RRB, we only performed statistical comparisons and neuroimaging correlations with scores from ADI-R section C, which pertain to RRB. We used a general linear model to explore the main effect of sex on ADI-R section C scores while covarying for age.

Basal ganglia and cerebellar volumes

We assessed basal ganglia and cerebellar volumes using ROIs from well-established atlases of the basal ganglia [39, 40] and cerebellum [41, 42]. We evaluated both left and right hemisphere ROIs in the basal ganglia and cerebellum, as well as midline structures in the cerebellum. We evaluated a total of 14 basal ganglia ROIs and 34 cerebellar ROIs (see Table 2).

ROIs were transformed from MNI space to participant space in order to assess volume of each ROI while accounting for total brain volume of the participant. Structural scans from each participant were corrected for signal inhomogeneity and non-linearly registered to MNI space using Advanced Normalization Tools (ANTs) [43]. ROIs were transformed from MNI space to individual participant space using the inverse transformation matrix between the participant and MNI space. For each participant, total volume of each ROI was divided by the total brain volume for that participant, so that ROI volumes were represented as a percent total brain volume. A 2×2 ANCOVA was used to assess the effects of diagnosis and sex on percent total brain volume for each of the 48 ROIs, using age and MRI scanner as covariates. We also performed a supplementary analysis for each ROI as absolute volume (mm^3) using a 2×2 ANCOVA with factors of diagnosis and sex, covarying for age, MRI scanner, and total brain volume (in mm^3). Correction for multiple comparisons was performed using the false discovery rate (FDR) method [44].

Free-water and diffusion tensor imaging

Removal of non-CNS tissue was performed with FSL's Brain Extraction Tool (BET) on the first b_0 image and then applied to all remaining diffusion-weighted volumes. Diffusion-weighted scans were corrected for motion and eddy current distortions using affine registration to a reference volume (first b_0 image) with the eddy correct function in FSL. Data from FSL's eddy correct function was then used to rotate the diffusion-weighting directions (i.e., b -vectors), in order to properly estimate the diffusion tensor and diffusion parameters in each voxel after correcting for the distortions caused by motion and eddy currents. Motion was characterized

relative to the b_0 image for each diffusion-weighted volume. For each diffusion-weighted volume, a summary measure of the total movement across all intracerebral voxels volume was calculated by taking displacement of each voxel and then averaging the squares of those displacements (i.e., root mean square). After applying the initial motion exclusion criteria described under Participant Data (i.e., more than 25% of volumes with >2 mm motion), we then sought to compare the remaining participant's motion during diffusion MRI. For each participant, motion across all diffusion-weighted volumes was averaged to arrive at a single motion parameter. We compared motion between ASD and TD groups using a 2×2 ANCOVA with the factors of diagnosis and sex, covaried for age and MRI scanner.

We then quantified FW and corrected DTI scalar measures accordingly. FW was calculated using a custom MATLAB script based on Pasternak et al. [13], as described in previous work from our research group [15, 18, 45–49]. We then performed tensor element reconstruction with the DTIFIT function in FMRIB's Diffusion Toolbox (FDT) to generate free-water corrected fractional anisotropy (FA_T) maps for each participant. Figure 1 shows uncorrected fractional anisotropy (FA), corrected FA_T , and FW images from a representative participant in this dataset. We evaluated the following tracts in both left and right hemispheres: (1) Dorsolateral prefrontal cortex (DLPFC) to caudate; (2) Primary motor cortex, upper-extremity (M1-U) to putamen; (3) Substantia nigra (SN) to putamen; (4) Globus pallidus externa (GPe) to subthalamic nucleus (STN); (5) Superior cerebellar peduncle (SCP) to M1-U (see Fig. 2). Templates for the white matter tracts of interest were generated using identical methods to those described in previous work [48, 50, 51]. Briefly, tract templates were generated using probabilistic tractography in the FMRIB software library (FSL; probtrackx2) with slice-level thresholding on high-resolution diffusion imaging data from 100 participants (54 males, 46 females) included in the Human Connectome Project [52]. Seed and target masks were derived from ROIs included the Human Motor Area Template and well-established atlases of the basal ganglia [39, 40, 53, 54]. In the cerebellum, we focused on the SCP tract because prior research showed reduced FA in the SCP of individuals with ASD, which was correlated with motor deficits [55]. FW and FA_T were evaluated for both the left and right hemispheres for each of these five tracts, resulting in a total of 10 tracts. We also provide a supplementary analysis of uncorrected FA values in these same tracts.

A 2×2 ANCOVA was used to assess the effects of diagnosis (ASD or TD) and sex on FA_T and FW for each of the 10 tracts, using age and MRI scanner as

Table 2 Basal ganglia and cerebellar volumes

Region of interest	% Total brain volume Mean ± Stdev		Diagnosis		Sex		Diagnosis * Sex	
	ASD	TD	<i>P</i> _{raw}	<i>P</i> _{FDR}	<i>P</i> _{raw}	<i>P</i> _{FDR}	<i>P</i> _{raw}	<i>P</i> _{FDR}
Caudate (L)	2.13E-01 ± 3.24E-02	2.15E-01 ± 3.41E-02	0.525	0.664	< 0.001	***< 0.001	0.427	0.558
Caudate (R)	2.00E-01 ± 3.17E-02	2.03E-01 ± 3.32E-02	0.283	0.467	< 0.001	***< 0.001	0.161	0.464
Putamen (L)	3.55E-01 ± 5.31E-02	3.66E-01 ± 5.09E-02	0.042	0.277	< 0.001	***< 0.001	0.020	0.238
Putamen (R)	3.45E-01 ± 5.34E-02	3.55E-01 ± 5.14E-02	0.036	0.277	< 0.001	***< 0.001	0.015	0.238
Nucleus accumbens (L)	7.94E-02 ± 1.12E-02	8.10E-02 ± 1.08E-02	0.126	0.301	< 0.001	***< 0.001	0.112	0.453
Nucleus accumbens (R)	7.65E-02 ± 1.10E-02	7.89E-02 ± 1.12E-02	0.025	0.277	< 0.001	***< 0.001	0.113	0.453
Globus pallidus external (L)	6.49E-02 ± 1.03E-02	6.63E-02 ± 9.75E-03	0.208	0.411	< 0.001	***< 0.001	0.017	0.238
Globus pallidus external (R)	5.98E-02 ± 9.80E-03	6.13E-02 ± 8.91E-03	0.150	0.327	< 0.001	***< 0.001	0.038	0.258
Globus pallidus internal (L)	2.36E-02 ± 4.07E-03	2.40E-02 ± 3.85E-03	0.271	0.465	< 0.001	***< 0.001	0.006	0.238
Globus pallidus internal (R)	2.20E-02 ± 3.69E-03	2.32E-02 ± 3.92E-03	0.019	0.277	< 0.001	***< 0.001	0.037	0.258
Subthalamic nucleus (L)	5.24E-03 ± 9.61E-04	5.36E-03 ± 1.10E-03	0.419	0.609	< 0.001	***< 0.001	0.139	0.464
Subthalamic nucleus (R)	5.19E-03 ± 9.53E-04	5.16E-03 ± 1.00E-03	0.804	0.839	< 0.001	***< 0.001	0.850	0.850
Substantia nigra (L)	1.19E-02 ± 1.81E-03	1.22E-02 ± 2.03E-03	0.292	0.467	0.003	**0.004	0.138	0.464
Substantia nigra (R)	1.20E-02 ± 1.81E-03	1.24E-02 ± 2.05E-03	0.112	0.301	< 0.001	***< 0.001	0.040	0.258
Lobule I-IV (L)	2.80E-01 ± 4.96E-02	2.82E-01 ± 4.75E-02	0.547	0.673	0.029	*0.031	0.381	0.558
Lobule I-IV (R)	2.91E-01 ± 5.22E-02	2.95E-01 ± 4.60E-02	0.459	0.623	0.020	*0.022	0.252	0.504
Lobule V (L)	3.30E-01 ± 5.39E-02	3.40E-01 ± 5.16E-02	0.113	0.301	< 0.001	**0.001	0.390	0.558
Lobule V (R)	3.37E-01 ± 5.82E-02	3.48E-01 ± 5.28E-02	0.105	0.301	0.006	**0.008	0.432	0.558
Lobule VI (L)	6.28E-01 ± 1.15E-01	6.60E-01 ± 8.94E-02	0.023	0.277	0.002	**0.003	0.510	0.627
Lobule VI (vermis)	1.51E-01 ± 3.19E-02	1.56E-01 ± 3.01E-02	0.230	0.425	0.002	**0.002	0.228	0.504
Lobule VI (R)	5.58E-01 ± 9.53E-02	5.86E-01 ± 9.04E-02	0.018	0.277	< 0.001	***< 0.001	0.523	0.627
Crus I (L)	1.02 ± 1.61E-01	1.05 ± 1.53E-01	0.069	0.277	< 0.001	***< 0.001	0.832	0.850
Crus I (vermis)	1.14E-03 ± 3.41E-04	1.16E-03 ± 3.55E-04	0.580	0.696	< 0.001	**0.001	0.113	0.453
Crus I (R)	1.02 ± 1.44E-01	1.06 ± 1.50E-01	0.038	0.277	< 0.001	***< 0.001	0.221	0.504
Crus II (L)	7.64E-01 ± 1.15E-01	7.70E-01 ± 1.35E-01	0.408	0.609	< 0.001	***< 0.001	0.292	0.540
Crus II (vermis)	3.63E-02 ± 7.70E-03	3.80E-02 ± 7.77E-03	0.062	0.277	< 0.001	**0.001	0.365	0.558
Crus II (R)	7.32E-01 ± 1.09E-01	7.49E-01 ± 1.23E-01	0.115	0.301	< 0.001	***< 0.001	0.105	0.453
Lobule VIIb (L)	3.57E-01 ± 5.39E-02	3.53E-01 ± 5.05E-02	0.859	0.877	< 0.001	***< 0.001	0.164	0.464
Lobule VIIb (vermis)	1.28E-02 ± 2.93E-03	1.34E-02 ± 2.66E-03	0.127	0.301	0.005	**0.006	0.539	0.631
Lobule VIIb (R)	3.81E-01 ± 5.49E-02	3.80E-01 ± 5.22E-02	0.740	0.790	< 0.001	***< 0.001	0.043	0.258
Lobule VIIa (L)	3.95E-01 ± 6.30E-02	3.88E-01 ± 5.36E-02	0.660	0.773	0.001	**0.002	0.200	0.504
Lobule VIIa (vermis)	8.75E-02 ± 1.55E-02	8.92E-02 ± 1.68E-02	0.414	0.609	0.007	**0.009	0.331	0.558
Lobule VIIa (R)	3.53E-01 ± 5.34E-02	3.48E-01 ± 4.67E-02	0.712	0.778	0.009	*0.010	0.234	0.504
Lobule VIIIb (L)	3.42E-01 ± 5.20E-02	3.40E-01 ± 4.61E-02	0.999	0.999	0.049	*0.050	0.842	0.850
Lobule VIIIb (vermis)	4.29E-02 ± 7.65E-03	4.44E-02 ± 8.73E-03	0.112	0.301	0.001	**0.002	0.397	0.558
Lobule VIIIb (R)	3.34E-01 ± 5.50E-02	3.29E-01 ± 4.57E-02	0.714	0.778	0.221	0.221	0.820	0.850
Lobule IX (L)	2.59E-01 ± 4.33E-02	2.61E-01 ± 4.82E-02	0.701	0.778	0.015	*0.018	0.389	0.558
Lobule IX (vermis)	5.66E-02 ± 9.18E-03	5.81E-02 ± 9.38E-03	0.214	0.411	0.004	**0.006	0.164	0.464
Lobule IX (R)	2.59E-01 ± 4.30E-02	2.63E-01 ± 4.68E-02	0.451	0.623	0.032	*0.033	0.418	0.558
Lobule X (L)	6.37E-02 ± 1.09E-02	6.63E-02 ± 9.48E-03	0.059	0.277	< 0.001	**0.001	0.572	0.638
Lobule X (vermis)	2.71E-02 ± 5.09E-03	2.76E-02 ± 5.07E-03	0.494	0.641	0.009	*0.010	0.559	0.638
Lobule X (R)	5.37E-02 ± 9.79E-03	5.49E-02 ± 8.64E-03	0.261	0.463	< 0.001	***< 0.001	0.442	0.558
Dentate nucleus (L)	9.67E-02 ± 1.63E-02	1.00E-01 ± 1.53E-02	0.067	0.277	< 0.001	***< 0.001	0.337	0.558
Dentate nucleus (R)	1.06E-01 ± 1.84E-02	1.10E-01 ± 1.67E-02	0.113	0.301	< 0.001	***< 0.001	0.253	0.504
Interposed nucleus (L)	1.19E-02 ± 2.26E-03	1.22E-02 ± 1.97E-03	0.210	0.411	< 0.001	***< 0.001	0.323	0.558
Interposed nucleus (R)	1.23E-02 ± 2.39E-03	1.28E-02 ± 2.43E-03	0.132	0.301	< 0.001	***< 0.001	0.178	0.476
Fastigial nucleus (L)	4.05E-03 ± 8.35E-04	4.13E-03 ± 8.28E-04	0.467	0.623	0.028	*0.031	0.700	0.763
Fastigial nucleus (R)	3.20E-03 ± 6.86E-04	3.37E-03 ± 7.15E-04	0.047	0.277	< 0.001	***< 0.001	0.262	0.504

Table 2 (continued)

Group means (\pm StDev), raw p values, and FDR corrected p values from 2×2 ANCOVA of basal ganglia and cerebellar volumes, as a percent of total brain volume, covaried for age and MRI scanner. Significant FDR corrected p values are bolded and indicated by * $p < 0.05$; ** $p < 0.01$; *** $p < 0.001$. All ROIs with significant sex differences were female > male percent of total brain volumes

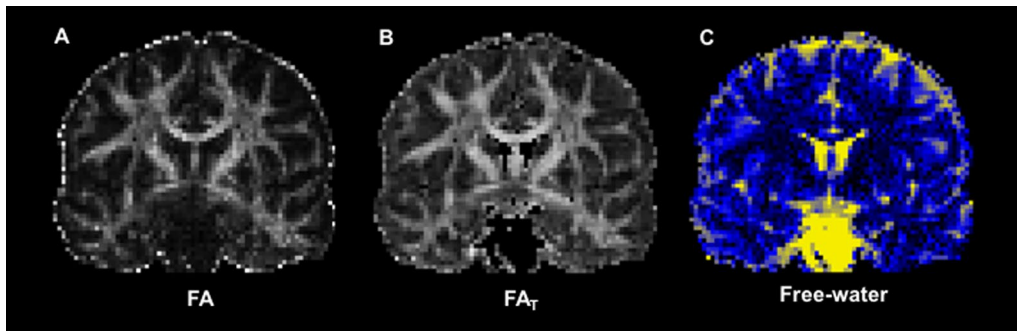


Fig. 1 Representative images for diffusion measures. Diffusion imaging data for **A** uncorrected fractional anisotropy (FA), **B** free-water corrected fractional anisotropy (FA_T), and **C** free-water from a representative TD participant

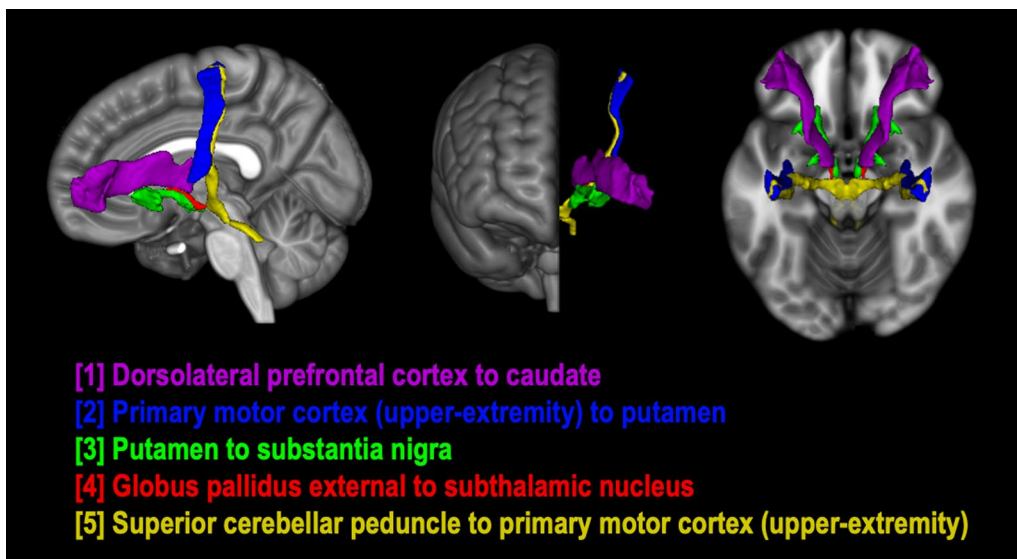


Fig. 2 Basal ganglia and cerebellar white matter tracts of interest. Three-dimensional rendering of white matter tract templates depicted from lateral (left), anterior (center), and superior (right) viewpoints. Tracts between the following brain regions were included: (1) Dorsolateral prefrontal cortex to caudate—purple; (2) Primary motor cortex (upper-extremity) to putamen—blue; (3) Substantia nigra to putamen—green; (4) Globus pallidus externa to subthalamic nucleus—red; (5) Superior cerebellar peduncle to primary motor cortex (upper-extremity)—yellow. These tracts were subdivided along the midline into left and right hemispheres for diffusion MRI analyses

covariates. Correction for multiple comparisons was performed with FDR, implemented separately for FA_T and FW measures. Next, significant whole-tract differences were followed with slice-level analysis to determine differences in FA_T and FW in each slice along the tract. A custom Linux shell-script computed the average FA_T and FW at each slice along the primary axis of travel for the tract. These slice-level averages were then compared between ASD and TD groups using

independent samples t-tests with FDR correction, similar to previous work [50].

Brain-behavior correlations

We performed correlations to assess the association of clinical measures of RRB with basal ganglia and cerebellar volumes, as well as FA_T and FW in the white matter tracts. RBS-R scores were available for both the ASD ($n = 82$) and TD ($n = 93$) participants and were

correlated with imaging measures using Spearman's Rho, as the distribution of scores was non-normal. Repetitive behavior scores from section C of the ADI-R, were only available from individuals from the ASD group, and thus correlations for the ADI-R were only preformed within the ASD group. Correction for multiple comparisons was performed with FDR, implemented separately volume, FA_T , and FW correlations.

Results

Demographic data and clinical scales

For IQ scores, there was a significant main effect of diagnosis ($F_{1,183}=7.97$, $p=0.005$), no main effect of sex, and no interaction between diagnosis and sex. Post-hoc tests showed that the ASD group had lower IQ scores than the TD group (Table 1). Regarding participant age, there was no main effect of diagnosis or sex, nor interaction between diagnosis and sex.

For the RBS-R, there was a significant main effect of diagnosis on RBS-R total score ($F_{1,171}=114$, $p<0.001$), no main effect of sex, and no interaction between diagnosis and sex. The ASD group had higher RBS-R total scores than the TD group (Table 1). Main effects of diagnosis were also seen for the RBS-R subscales of stereotyped behavior ($F_{1,171}=62.3$, $p<0.001$), self-injurious behavior ($F_{1,171}=41.1$, $p<0.001$), compulsive behavior ($F_{1,171}=42.4$, $p<0.001$), ritualistic behavior ($F_{1,171}=77.9$, $p<0.001$), sameness behavior ($F_{1,171}=77.9$, $p<0.001$). For all subscales, the ASD group had higher scores than the TD group. No main effects of sex, and no interactions between diagnosis and sex were found for these RBS-R subscales.

For the restricted interests subscale there was both a main effect of diagnosis ($F_{1,171}=114$, $p<0.001$), a main effect of sex ($F_{1,171}=22.1$, $p<0.001$), and an interaction between diagnosis and sex ($F_{1,171}=14.6$, $p<0.001$). Post-hoc tests on the restricted interests subscale revealed that males had significantly higher scores than females in both the ASD group ($F_{1,81}=17.8$, $p<0.001$) and TD group ($F_{1,90}=4.15$, $p=0.045$), although this sex difference was more pronounced in the ASD group.

For the SCQ, there was a main effect of diagnosis ($F_{1,180}=394$, $p<0.001$), with the ASD group having significantly higher SCQ scores than the TD group. There was also a main effect of sex ($F_{1,180}=10.6$, $p=0.001$), such that males had higher SCQ scores than females. There was no significant interaction between diagnosis and sex.

Scores from section C of the ADI-R were only available for individuals in the ASD group. There was a no effect of sex on ADI-R section C scores.

Basal ganglia and cerebellar volumes

For ROIs of the basal ganglia and cerebellum, there were no significant main effects of diagnosis, nor interactions between diagnosis and sex on regional gray matter volumes after FDR correction. This was the case whether ROI volume was compared as a percent of total brain volume (Table 2) or as absolute volume (in mm^3) and covaried by the participant's total brain volume (Additional file 1: Table S1).

The main effect of sex, which applied equally to both ASD and TD groups, differed between these two approaches for comparing volume. When ROI volume was compared as a percentage of total brain volume, there was a significant main effect of sex ($p_{FDR}<0.05$) for all ROIs except for right lobule VIIIb, where females had larger percent total brain volume than males in these ROIs (Table 2). When volumes were compared in mm^3 and covaried by total brain volume (Additional file 1: Table S1), there were fewer ROIs that showed a significant main effect of sex ($p_{FDR}<0.05$), all of which showed males had larger absolute volume of these structures (due to larger total brain volume male participants): Lobule I–IV (L and R), Lobule V (L and R), Lobule VIIa (L and R), and Lobule VIIIb (L and R).

Free-water and diffusion tensor imaging

When comparing head motion between groups, after the initial exclusion criteria for major motion artifacts was applied (i.e., participant excluded if more than 25% of volumes had >2 mm motion), there was no significant effect of diagnosis ($F_{1,166}=1.08$, $p=0.301$), sex ($F_{1,166}=0.649$, $p=0.422$), nor interaction between diagnosis and sex ($F_{1,166}=0.198$, $p=0.657$) on motion during diffusion MRI.

For FA_T , there was a significant FDR corrected main effect of diagnosis on the DLPFC to caudate (L) tract ($F_{1,166}=11.8$, $p_{FDR}=0.008$), which showed lower FA_T in ASD participants. This tract was further investigated using slice-level thresholding, which revealed that slices with significantly lower FA_T in ASD participants ($p_{FDR}<0.05$) were proximal to the caudate (Fig. 3). Although there was no significant interaction between diagnosis and sex for FA_T in any of the tracts evaluated, there was a significant FDR corrected main effect of sex for tracts between SN to putamen (L) ($F_{1,166}=11.64$, $p_{FDR}=0.004$) and SN to putamen (R) ($F_{1,166}=20.8$, $p_{FDR}<0.001$), as well as GPe to STN (L) ($F_{1,166}=8.50$, $p_{FDR}=0.014$) and GPe to STN (R) ($F_{1,166}=6.34$, $p_{FDR}=0.032$), all of which showed lower FA_T in females than males in both ASD and TD groups. Table 3 summarizes tract average FA_T findings.

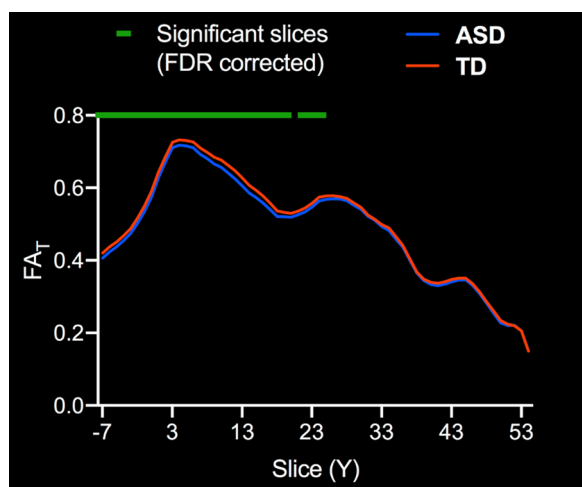


Fig. 3 Slice-level analysis of FA_T in white matter tracts with significant effect of diagnosis. Slice-level analysis of free-water corrected fractional anisotropy (FA_T) for the left hemisphere dorsolateral prefrontal cortex to caudate tract (DLPFC to Caudate). Group means for ASD (blue) and TD groups (orange) are depicted. The green line indicates slices with significant differences between groups, FDR corrected for multiple comparisons. Slice numbers in the anterior–posterior (Y) plane are in Talairach coordinates

The supplementary analysis of uncorrected FA values similarly showed a significant FDR adjusted main effects of diagnosis in the DLPFC to caudate (L) tract ($F_{1,166} = 21.0, p_{FDR} < 0.001$) but also in the DLPFC to caudate (R) tract ($F_{1,166} = 12.1, p_{FDR} < 0.01$). There was a significant main effect of sex for the tracts M1U to caudate (L) ($F_{1,166} = 17.7, p_{FDR} < 0.001$) and M1U to caudate (R) ($F_{1,166} = 10.8, p_{FDR} < 0.01$), as well as GPe to STN (L) ($F_{1,166} = 11.5, p_{FDR} < 0.01$) and GPe to STN (R) ($F_{1,166} = 12.1, p_{FDR} < 0.01$). There was no significant interaction between diagnosis and sex on uncorrected

FA in any of the tracts evaluated. Additional file 1: Table S2 summarizes the tract average findings for uncorrected FA.

For FW, there was a significant FDR corrected main effect of diagnosis for DLPFC to caudate (L) ($F_{1,166} = 9.68, p_{FDR} = 0.011$) and DLPFC to caudate (R) ($F_{1,166} = 5.89, p_{FDR} = 0.041$), SN to putamen (L) ($F_{1,166} = 10.2, p_{FDR} = 0.011$), and GPe to STN (L) ($F_{1,166} = 6.90, p_{FDR} = 0.031$), all of which showed greater FW in ASD participants. These tracts were further investigated using slice-level thresholding. For DLPFC to caudate tracts, slices that had significantly higher FW ($p_{FDR} < 0.05$) were those proximal to both caudate and DLPFC (Fig. 4A, B). For SN to putamen (L), slices that had significantly higher FW ($p_{FDR} < 0.05$) were primarily those in the middle of the tract (Fig. 4C). For GPe to STN (L), slices that had significantly higher FW ($p_{FDR} < 0.05$) occurred proximal to both GPe and STN (Fig. 4C). There were no significant main effects of sex on FW for any of the tracts investigated, nor were there significant interactions between diagnosis and sex on FW. Table 4 summarizes tract average FW findings.

Brain-behavior correlations

We observed no significant FDR corrected correlations between volume of structures in the basal ganglia and cerebellum with ADI-R Section C scores or SCQ scores. There was a significant negative correlation between RBS-R total score and volume of cerebellar lobule VI (L) ($R = -0.25, p_{FDR} < 0.05$). There were no significant FDR corrected correlations between RBS-R subscale scores and volume for any of the structures measured. Correlations between volume and behavioral measures are depicted in Additional file 1: Table S3.

Table 3 Fractional anisotropy (free-water corrected) in basal ganglia and cerebellar white matter tracts

Tract FA _T	Mean ± Stdev		Diagnosis		Sex		Diagnosis*sex	
	ASD	TD	<i>p</i> _{raw}	<i>p</i> _{FDR}	<i>p</i> _{raw}	<i>p</i> _{FDR}	<i>p</i> _{raw}	<i>p</i> _{FDR}
DLPFC to Caudate (L)	0.441 ± 0.014	0.450 ± 0.017	0.001	*0.008	0.069	0.114	0.772	0.956
DLPFC to Caudate (R)	0.409 ± 0.017	0.415 ± 0.017	0.014	0.063	0.032	0.063	0.255	0.956
M1U to Putamen (L)	0.403 ± 0.016	0.406 ± 0.020	0.290	0.322	0.527	0.585	0.675	0.956
M1U to Putamen (R)	0.399 ± 0.017	0.401 ± 0.022	0.367	0.367	0.810	0.810	0.313	0.956
SCP to M1U (L)	0.534 ± 0.014	0.537 ± 0.016	0.251	0.314	0.273	0.363	0.694	0.956
SCP to M1U (R)	0.520 ± 0.015	0.524 ± 0.019	0.082	0.165	0.290	0.363	0.956	0.956
SN to Putamen (L)	0.417 ± 0.016	0.422 ± 0.018	0.108	0.181	0.001	**0.004	0.480	0.956
SN to Putamen (R)	0.405 ± 0.017	0.409 ± 0.020	0.152	0.218	<0.001	***<0.001	0.371	0.956
GPe to STN (L)	0.558 ± 0.019	0.566 ± 0.025	0.045	0.114	0.004	*0.014	0.460	0.956
GPe to STN (R)	0.573 ± 0.023	0.584 ± 0.028	0.019	0.063	0.013	*0.032	0.928	0.956

Group means (± StDev), raw *p* values, and FDR corrected *p* values from 2 × 2 ANCOVA for free-water corrected fractional anisotropy (FA_T) in each white matter tract, covaried for age and MRI scanner. Significant FDR corrected *p* values are bolded and indicated by **p* < 0.05; ***p* < 0.01; ****p* < 0.001

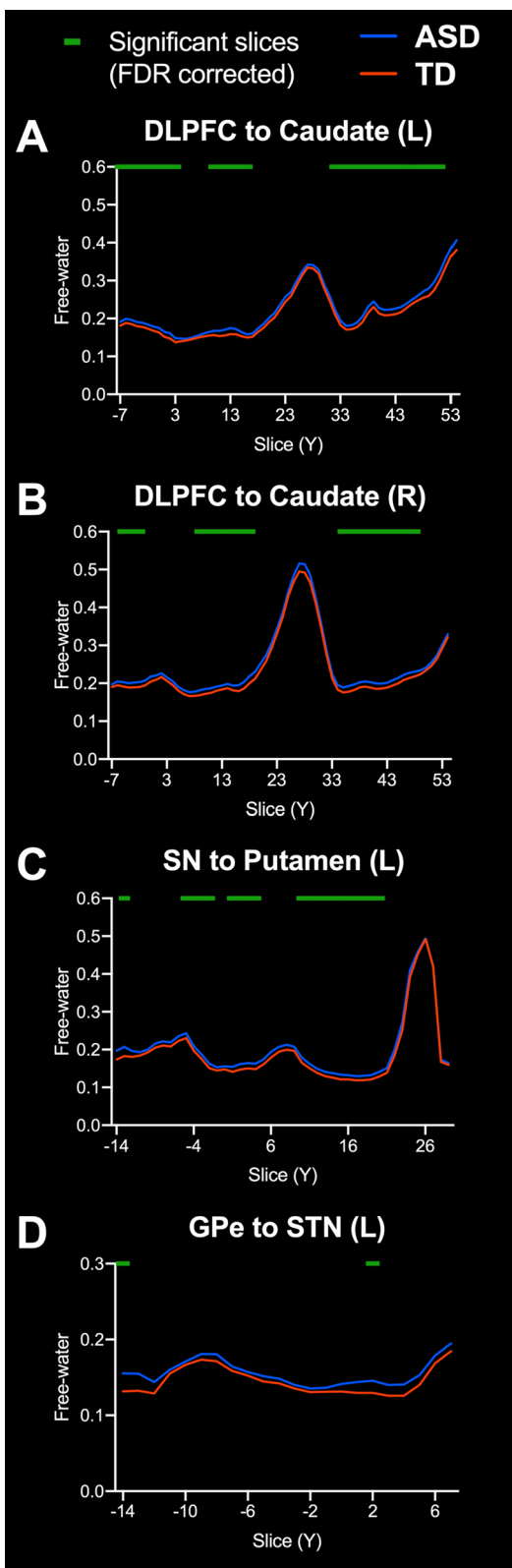


Fig. 4 Slice-level analysis of free-water in white matter tracts with a significant effect of diagnosis. Slice-level analysis of free-water (FW) for the **A** left hemisphere dorsolateral prefrontal cortex to caudate (DLPFC to Caudate) tract, **B** right hemisphere DLPFC to caudate tract, **C** left hemisphere substantia nigra to putamen (SN to putamen) tract, and **D** left hemisphere globus pallidus externa to subthalamic nucleus (GPe to STN) tract. Group means for ASD (blue) and TD groups (orange) are depicted. The green line indicates slices with significant differences between groups, FDR corrected for multiple comparisons. Slice numbers in the anterior–posterior (Y) plane are in Talairach coordinates

For FA_T , there was a significant negative correlation between DLPFC to caudate (*L*) tract FA_T and RBS-R total score ($R = -0.28, p_{FDR} = 0.003$), as well as subscales for stereotyped behavior ($R = -0.24, p_{FDR} = 0.028$), ritualistic behavior ($R = -0.22, p_{FDR} = 0.043$), sameness behavior ($R = -0.27, p_{FDR} = 0.005$), and restricted interests ($R = -0.27, p_{FDR} = 0.005$). There was also significant negative correlation between FA_T in the DLPFC to caudate (*R*) tract and the RBS-R stereotyped behavior ($R = -0.22, p_{FDR} = 0.028$) and restricted interests subscales ($R = -0.22, p_{FDR} = 0.026$). For the SN to putamen (*L*) tract there were significant negative correlation between FA_T and the RBS-R subscale for restricted interests ($R = -0.20, p_{FDR} = 0.039$). For the GPe to STN (*R*) tract there was a significant negative correlation between FA_T and the RBS-R subscale for sameness behavior ($R = -0.21, p_{FDR} = 0.036$). Raw and FDR corrected *p* values for correlations between tract FA_T and ADI-R section C, RBS-R total score, and RBS-R subscales are included in Table 5.

The supplementary analysis of correlating uncorrected FA values against behavioral measures showed a significant negative correlation between DLPFC to caudate (*L*) tract uncorrected FA and RBS-R total score ($R = -0.35, p_{FDR} < 0.001$), as well as subscales for stereotyped behavior ($R = -0.30, p_{FDR} < 0.001$), compulsive behavior ($R = -0.25, p_{FDR} < 0.05$), ritualistic behavior ($R = -0.32, p_{FDR} < 0.001$), sameness behavior ($R = -0.30, p_{FDR} < 0.001$), and restricted interests ($R = -0.39, p_{FDR} < 0.001$). There was also a significant negative correlation between DLPFC to caudate (*R*) tract uncorrected FA and RBS-R total score ($R = -0.27, p_{FDR} < 0.01$), as well as subscales for stereotyped behavior ($R = -0.29, p_{FDR} < 0.001$), ritualistic behavior ($R = -0.22, p_{FDR} < 0.05$), sameness behavior ($R = -0.25, p_{FDR} < 0.01$), and restricted interests ($R = -0.36, p_{FDR} < 0.001$). Unlike corrected FA_T , there was also a significant correlation between uncorrected FA and SCQ scores for the DLPFC to caudate (*L*) ($R = -0.28, p_{FDR} < 0.01$) and DLPFC to caudate (*R*) ($R = -0.21, p_{FDR} < 0.05$) tracts. Correlations between uncorrected FA and behavioral measures are depicted in Additional file 1: Table S4.

Table 4 Free-water in basal ganglia and cerebellar white matter tracts

Tract FW	Mean ± Stdev		Diagnosis		Sex		Diagnosis * sex	
	ASD	TD	<i>p</i> _{raw}	<i>p</i> _{FDR}	<i>p</i> _{raw}	<i>p</i> _{FDR}	<i>p</i> _{raw}	<i>p</i> _{FDR}
DLPFC to Caudate (L)	0.227 ± 0.028	0.214 ± 0.025	0.002	*0.011	0.501	0.974	0.733	0.987
DLPFC to Caudate (R)	0.244 ± 0.037	0.230 ± 0.032	0.016	*0.041	0.920	0.974	0.533	0.987
M1U to Putamen (L)	0.205 ± 0.041	0.206 ± 0.052	0.611	0.763	0.507	0.974	0.632	0.987
M1U to Putamen (R)	0.212 ± 0.040	0.211 ± 0.047	0.915	0.915	0.974	0.974	0.291	0.727
SCP to M1U (L)	0.184 ± 0.027	0.185 ± 0.033	0.601	0.763	0.862	0.974	0.987	0.987
SCP to M1U (R)	0.197 ± 0.031	0.195 ± 0.030	0.914	0.915	0.724	0.974	0.945	0.987
SN to Putamen (L)	0.175 ± 0.024	0.164 ± 0.019	0.002	*0.011	0.633	0.974	0.282	0.727
SN to Putamen (R)	0.196 ± 0.029	0.185 ± 0.027	0.049	0.098	0.577	0.974	0.198	0.727
GPe to STN (L)	0.156 ± 0.029	0.145 ± 0.022	0.009	*0.031	0.361	0.974	0.224	0.727
GPe to STN (R)	0.165 ± 0.030	0.159 ± 0.031	0.344	0.574	0.635	0.974	0.793	0.987

Group means (± StDev), raw *p* values, and FDR corrected *p* values from 2 × 2 ANCOVA for free-water (FW) in each white matter tract, covaried for age and MRI scanner. Significant FDR corrected *p* values are bolded and indicated by **p* < 0.05, ***p* < 0.01, ****p* < 0.001

For FW, there was a significant positive correlation between DLPFC to caudate (L) tract FW with the RBS-R restricted interests subscale ($R=0.23$, $p_{FDR}=0.021$) and the SCQ score ($R=0.25$, $p_{FDR}=0.006$). For the DLPFC to caudate (R) tract FW there were also significant positive correlations with RBS-R restricted interests subscale ($R=0.22$, $p_{FDR}=0.021$) and SCQ score ($R=0.21$, $p_{FDR}=0.013$). For the SN to putamen (L) tract there was a significant positive correlation between FW and SCQ score ($R=0.26$, $p_{FDR}=0.006$). For the GPe to STN (L) tract there was a significant positive correlation between FW and SCQ score ($R=0.22$, $p_{FDR}=0.013$). Raw and FDR corrected *p* values for correlations between tract FW and ADI-R section C, RBS-R total score, and RBS-R subscales are included in Table 6.

Discussion

There has been relatively limited focus on morphological and connectivity differences associated with RRB in ASD. An approach frequently employed to assess brain-behavior relationships to RRB in ASD has been correlation of regional gray matter volumes with clinical scales [56–62]. Other work has used fMRI to assess activation or functional connectivity as it relates to RRB [63–71]. Fewer studies, however, have used diffusion imaging to assess white matter correlates of RRB [64, 66, 72–74]. Adding complexity to this line of inquiry, there is mixed evidence regarding sex differences in expression of RRB in ASD [32–36]. Relatively few studies have examined sex differences in ASD using diffusion imaging, and none of these studies investigated the relationship of such findings with RRB [28, 29, 75, 76]. In this study we assessed measures of RRB, regional gray matter volumes and white matter microstructure in the basal ganglia and cerebellum in a large cohort of ASD and TD individuals, with nearly

equal numbers of males and females in each group. We also evaluated whether biological sex interacted with ASD diagnosis on these neuroimaging outcome measures, and their relationship to RRB. To our knowledge, this work is the first to assess microstructure of intra-basal ganglia white matter pathways (i.e., SN to putamen, GPe to STN) in ASD and how such pathways relate to expression of RRB. This study is also among the first to quantify FW or implement free-water correction of DTI data in ASD [20, 21].

We observed higher levels of RRB in individuals with ASD, as expected. Overall patterns of RRB were similar between males and females with ASD, as the ADI-R section C and RBS-R total score showed no significant sex differences. There was, however, a significant diagnosis by sex interaction for the restricted interests subscale of the RBS-R. This specific finding regarding restricted interests is in line with other studies that have used the RBS-R to investigate sex differences in the expression of RRB in ASD [34, 36]. We also observed that within TD participants, males showed higher scores on the restricted interests subscale, but this effect was less pronounced than in ASD participants.

Our neuroimaging findings suggest that the gray matter volumes in the basal ganglia and cerebellum, adjusted for total brain volume, do not distinguish children and adolescents with ASD from their TD counterparts. We found no interaction between diagnosis and sex on volume of structures in the basal ganglia and cerebellum, although there were significant sex effects that applied equally to both ASD and TD groups. Previously reported volumetric differences in ASD and their relation to RRB may have been biased by inclusion of only males or very small numbers of females, as well as smaller sample sizes [56–59]. In a larger study of 472 individuals with ASD (54

Table 5 Brain-behavior correlations for fractional anisotropy (free-water corrected) in basal ganglia and cerebellar white matter tracts

Tract FA _r	ADI-R section C		RBS-R total		RBS-R stereotyped		RBS-R self-injury		RBS-R compulsive		RBS-R ritual		RBS-R sameness		RBS-R restricted interests		SCQ	
	<i>P</i> _{raw}	<i>P</i> _{FDR}	<i>P</i> _{raw}	<i>P</i> _{FDR}	<i>P</i> _{raw}	<i>P</i> _{FDR}												
DLPFC to Caudate (L)	0.500	0.930	<0.001	**0.003	0.004	*0.028	0.046	0.309	0.016	0.164	0.004	*0.043	<0.001	**0.005	0.001	**0.005	0.021	0.211
DLPFC to Caudate (R)	0.029	0.288	0.025	0.063	0.006	*0.028	0.062	0.309	0.437	0.534	0.189	0.315	0.032	0.089	0.005	*0.026	0.441	0.773
M1U to Putamen (L)	0.168	0.839	0.187	0.268	0.367	0.459	0.779	0.918	0.289	0.413	0.770	0.770	0.250	0.312	0.053	0.076	0.696	0.773
M1U to Putamen (R)	0.930	0.930	0.565	0.628	0.617	0.617	0.892	0.918	0.164	0.354	0.411	0.587	0.817	0.817	0.829	0.637	0.773	0.773
SCP to M1U (L)	0.817	0.930	0.322	0.403	0.513	0.570	0.393	0.786	0.481	0.534	0.649	0.722	0.082	0.117	0.243	0.304	0.799	0.799
SCP to M1U (R)	0.661	0.930	0.741	0.741	0.341	0.459	0.918	0.918	0.922	0.922	0.635	0.722	0.329	0.366	0.778	0.829	0.566	0.773
SN to Putamen (L)	0.919	0.930	0.020	0.063	0.067	0.130	0.138	0.461	0.118	0.354	0.015	0.066	0.039	0.089	0.012	*0.039	0.208	0.773
SN to Putamen (R)	0.334	0.930	0.068	0.114	0.065	0.130	0.228	0.569	0.212	0.354	0.020	0.066	0.049	0.089	0.050	0.076	0.481	0.773
GPe to STN (L)	0.894	0.930	0.054	0.109	0.078	0.130	0.899	0.918	0.164	0.354	0.063	0.127	0.053	0.089	0.037	0.076	0.429	0.773
GPe to STN (R)	0.727	0.930	0.023	0.063	0.033	0.111	0.770	0.918	0.178	0.354	0.030	0.076	0.007	*0.036	0.041	0.076	0.318	0.773

Raw and FDR corrected *p* values from Spearman correlations between free-water corrected fractional anisotropy (FA_r) in basal ganglia and cerebellar tracts and behavioral measures. Measures of RRB included Section C of the Autism Diagnostic Interview-Revised (ADI-R), as well Repetitive Behavior Scale-Revised (RBS-R) total score and subsection scores. The Social Communication Questionnaire (SCQ) measures social and communication behaviors. Significant FDR corrected *p* values are bolded and indicated by **p*<0.05, ***p*<0.01, ****p*<0.001

Table 6 Brain-behavior correlations for free-water in basal ganglia and cerebellar white matter tracts

Tract free-water	ADI-R section C		RBS-R total		RBS-R stereotyped		RBS-R self-injury		RBS-R compulsive		RBS-R ritual		RBS-R sameness		RBS-R restricted interests		SCQ	
	<i>P</i> _{raw}	<i>P</i> _{FDR}	<i>P</i> _{raw}	<i>P</i> _{FDR}	<i>P</i> _{raw}	<i>P</i> _{FDR}												
DLPFC to Caudate (L)	0.737	0.886	0.012	0.122	0.204	0.408	0.459	0.995	0.066	0.461	0.010	0.096	0.119	0.694	0.003	*0.021	0.001	**0.006
DLPFC to Caudate (R)	0.724	0.886	0.045	0.150	0.096	0.321	0.835	0.995	0.185	0.462	0.045	0.204	0.139	0.694	0.004	*0.021	0.005	*0.013
M1U to Putamen (L)	0.886	0.886	0.887	0.907	0.960	0.960	0.963	0.995	0.637	0.909	0.569	0.773	0.888	0.947	0.917	0.917	0.222	0.370
M1U to Putamen (R)	0.773	0.886	0.780	0.907	0.690	0.767	0.597	0.995	0.781	0.909	0.841	0.841	0.947	0.947	0.903	0.917	0.386	0.531
SCP to M1U (L)	0.208	0.886	0.907	0.907	0.398	0.569	0.581	0.995	0.835	0.909	0.812	0.841	0.664	0.947	0.687	0.858	0.502	0.558
SCP to M1U (R)	0.156	0.886	0.815	0.907	0.505	0.631	0.431	0.995	0.424	0.848	0.619	0.773	0.502	0.947	0.580	0.829	0.787	0.787
SN to Putamen (L)	0.807	0.886	0.035	0.150	0.082	0.321	0.735	0.995	0.138	0.461	0.061	0.204	0.334	0.834	0.025	0.082	0.001	**0.006
SN to Putamen (R)	0.504	0.886	0.289	0.578	0.171	0.408	0.995	0.995	0.618	0.909	0.283	0.567	0.754	0.947	0.128	0.257	0.054	0.108
GPe to STN (L)	0.668	0.886	0.070	0.174	0.041	0.321	0.783	0.995	0.127	0.461	0.204	0.510	0.291	0.834	0.105	0.257	0.004	*0.013
GPe to STN (R)	0.432	0.886	0.516	0.860	0.396	0.569	0.689	0.995	0.909	0.909	0.592	0.773	0.910	0.947	0.336	0.560	0.425	0.531

Raw and FDR corrected *p* values from Spearman correlations between free-water in basal ganglia and cerebellar tracts and behavioral measures. Measures of RRB included Section C of the Autism Diagnostic Interview-Revised (ADI-R), as well Repetitive Behavior Scale-Revised (RBS-R) total score and subsection scores. The Social Communication Questionnaire (SCQ) measures social and communication behaviors. Significant FDR corrected *p* values are bolded and indicated by **p* < 0.05, ***p* < 0.01, ****p* < 0.001

females), Turner et al. reported that individuals with ASD showed significant volumetric enlargement in the pallidum and lateral ventricles [77]. That study, however, did not investigate potential interactions between diagnosis and sex, but their results were identical when replicated in the male-only group. In a similar study of subcortical volume in 539 individuals with ASD (67 females), Zhang et al. found no effect of diagnostic group for any of the structures evaluated, nor any interaction between diagnosis and sex [30]. It is worth noting that both of those large studies included adults, whereas our study sample included only children and adolescents. There was a significant negative correlation between volume of cerebellar lobule VI (L) and RBS-R total score, an observation which matches Rojas et al. [58], where there was no volumetric difference between ASD and TD individuals in cerebellar lobule VI (L), but a significant negative correlation between repetitive behavior and volume of lobule VI (L) was reported.

In contrast, we found that microstructure of basal ganglia white matter tracts was significantly different in children and adolescents with ASD compared to TD participants. We found that individuals with ASD had lower FA_T in the DLPFC to caudate (L) tract, but there was no effect of sex, nor interaction between diagnosis and sex. We also found that individuals with ASD had higher FW in the DLPFC to caudate tracts (L and R), as well as tracts from SN to putamen (L) and GPe to STN (L), with no effect of sex nor interaction between diagnosis and sex. Lower FA_T in these tracts, excluding the GPe to STN (L) tract, were correlated with higher scores in at least one subscale of the RBS-R. Higher FW in DLPFC to caudate tracts (L and R) also correlated with higher RBS-R restricted interest scores. Although RBS-R total score and many RBS-R subscales were correlated with white matter microstructure, it is worth noting that no significant correlations were found between self-injury or compulsive behavior subscales with either FA_T or FW for any of the tracts examined.

The supplementary analysis of uncorrected FA values showed significant group differences in DLPFC to caudate tracts (L and R). Our objective in including this supplementary analysis is to provide an example of the different conclusions that may be arrived at when applying free-water quantification and correction to diffusion MRI data. In some of the evaluated tracts, such as GPe to STN, uncorrected FA values were nearly 40% greater than corresponding free-water corrected FA_T values. The relationship between FA and FA_T is determined on a voxel-by-voxel basis and is dependent on the FW fraction [13]. To illustrate the relationship between FA and FA_T in the context of this manuscript, we also provide correlations between tract-average FA and FA_T in Additional file 1:

Table S5. We believe it is especially relevant that the FW metric itself showed greater sensitivity at identifying significant differences between ASD and TD groups, which was observed in both DLPFC to caudate (L and R) tracts, as well as the in basal ganglia tracts SN to putamen (L) and GPe to STN (L).

In order to determine the specificity of these brain-behavior relationships to RRB we also performed correlations with the SCQ, which captures social and communication deficits seen in ASD, but also includes some items pertinent to RRB. There were no significant correlations between SCQ score and regional gray matter volumes in the basal ganglia and cerebellum, nor FA_T in the white matter tracts investigated. We found that higher SCQ scores correlated with higher FW in the DLPFC to caudate (L and R), SN to putamen (L), and GPe to STN (L) tracts. The supplementary analysis of uncorrected FA showed that DLPFC to caudate (L and R) was significantly correlated with nearly all RBS-R items as well as the SCQ, but no correlations were observed in other tracts. Considering RBS-R and SCQ findings together, evaluating uncorrected FA may lead to the conclusion that these white matter tracts reflect global severity of both RRB and social deficits. However, following free-water correction, FA_T was more specific to RRB and revealed novel involvement of basal ganglia pathways in the expression of RRB.

The DLPFC, which includes middle frontal gyrus and part of superior frontal gyrus [78–80], connects to the basal ganglia via the caudate [81]. Connections from DLPFC to the caudate are thought to play an important role in response inhibition [82]. Aberrant microstructure in the DLPFC to caudate white matter has been shown in other clinical populations with deficits in response inhibition, such as attention-deficit hyperactivity disorder [83] and obsessive-compulsive disorder [84]. Rojas et al. [58] found evidence for altered FA in white matter near the middle frontal gyrus (MFG) in ASD using a voxel-wise approach, but no prior tract-based study has identified aberrant microstructure in white matter connecting the DLPFC to caudate. A previous study in males with ASD found functional connectivity deficits between MFG and caudate, which was further correlated with RRB scores, but found no difference in FA for caudate tracts identified with tractography [64]. Another tractography study in males with ASD found lower FA in putamen tracts, but not in caudate tracts [66].

Quantification of free-water or corresponding correction of DTI scalars has had limited application in ASD research [20, 21]. It is possible that prior evaluations of basal ganglia white matter in ASD using FA as an outcome measure were impacted by partial volume effects of extracellular free-water. This consideration is especially

relevant for white matter tracts proximal to ventricles, such as the DLPFC to caudate tract. When we investigated FA_T of the DLPFC to caudate tract at slice-level, we found that the slices which had significantly lower FA_T in ASD were those most proximal to the ventricles (Fig. 3). The majority of these same DLPFC to caudate slices also had significantly higher FW in ASD (Fig. 4). We did not observe a main effect of sex, nor an interaction between diagnosis and sex, for either FA_T or FW in the DLPFC to caudate tract. FA_T in the DLPFC to caudate tract was negatively correlated with RBS-R total score and multiple subscales, whereas FW was positively correlated with the restricted interests RBS-R subscale. The supplementary analysis of uncorrected FA also showed significant group differences in ASD for the DLPFC to caudate tracts, and significant correlations for RBS-R and SCQ scores. Together these findings suggest altered microstructure of the DLPFC to caudate tract in ASD, and that higher rates of RRB are associated with greater disruption in this pathway.

The added value of FW imaging can also be seen in white matter pathways within the basal ganglia. Individuals with ASD had higher FW than TD individuals in the SN to putamen tract. Although we did not observe a group difference in FA_T for this SN to putamen tract, we found that FA_T was negatively correlated with the RBS-R restricted interests subscale. Projections from substantia nigra pars compacta (SNpc) to putamen provide dopaminergic tone to the striatum, and recurrent projections from putamen to SNpc provide regulatory feedback. Also connecting these regions, efferents from the putamen to substantia nigra pars reticulata (SNpr) are part the direct basal ganglia pathway. The SN target mask used in this study did not differentiate between the SNpr and SNpc. Consequently, we did not have the ability to differentiate whether the voxels represented in this tract were comprised of direct pathway GABAergic projections from putamen to SNpr, dopaminergic projections from SNpc to putamen, striosomal GABAergic recurrents from putamen to SNpc, or some combination of these.

Due to the multiple distinct white matter populations likely represented in the SN to putamen tract, there are multiple possible interpretations of the present findings for the SN to putamen tract. One possible interpretation is that there is impaired microstructure of the direct pathway in ASD associated with higher levels of RRB. Several theories surrounding RRB postulate an imbalance between direct and indirect pathways [85–87]. Prior studies do not provide evidence of direct pathway dysfunction associated with RRB in ASD, whereas the indirect pathway has been demonstrated to be an important mediator of RRB in work from animal models [87–93]. Another possible interpretation is that the

present findings reflect impaired nigrostriatal dopamine tone, due to projections from SNpc to putamen or striosomal recurrent projections from the putamen to SNpc. We find this interpretation more plausible, as nigrostriatal dopamine abnormalities have been hypothesized to underlie RRB in ASD [94]. Moreover, dopamine dysregulation has been linked to RRB in individuals with Parkinson's disease who receive dopamine replacement therapy, and is thought to relate to impaired activity of the indirect pathway [95, 96].

The GPe to STN tract (L) also had higher FW in individuals with ASD compared to TD participants. FW in the GPe to STN tracts did not correlate with RBS-R scores, but was found to have a positive correlation with SCQ scores. Although we did not observe a significant effect of diagnosis on FA_T in GPe to STN tracts, there was a significant negative correlation between FA_T in GPe to STN (R) and the RBS-R subscale for sameness behavior, which was further supported by trend level correlations with RBS-R total score and subscale for ritualistic behavior (see Table 6). Connections between the GPe and STN are specific to the indirect basal ganglia pathway, a pathway shown in animal studies to play a critical role in RRB [87–93]. Our findings in this tract support a role for the indirect pathway in ASD, as well as on the severity of RRB and social deficits as indexed by the RBS-R and SCQ, respectively.

A significant main effect of sex on FA_T was observed in the putamen to SN tracts (L and R), as well as GPe to STN tracts (L and R). In all of these tracts, males had higher FA_T than females. The greater FA_T observed in males for these basal ganglia pathways is consistent with a prior DTI investigation of sex differences in TD individuals during childhood and adolescence [97]. We did not observe an effect of sex on FW in any of the evaluated pathways. Importantly, there was no interaction between diagnosis and sex on either FA_T or FW for any of the investigated pathways, nor in the clinical scales evaluated in this study. Thus, the main effect of sex was not further explored in this study, as it applied to both ASD and TD populations equally. Nevertheless, other studies suggest that there may be sex differences in brain morphology or connectivity in ASD and it is important that future work in this area continue to evaluate sex as a factor [28, 98, 99].

The lack of significant diffusion imaging findings in cerebellar white matter tracts may be partially related to demographic differences in the study population compared to other similar work. Cheung et al. [73] previously reported a significant negative correlation between RRB and FA in cerebellar white matter. Their investigation included a smaller sample of 13 individuals with ASD, only 1 of which was female, and utilized the ADI-R

section C, which yielded no significant correlations in the present study. Regarding age, work has shown that children with ASD show dynamic changes in cerebellar white matter tracts across childhood that differ from their TD counterparts [100]. Moreover, altered FA in cerebellar pathways in infancy and toddlerhood has been associated with the later development of repetitive behaviors and autism. Wolff et al. [101] observed associations between RRB and FA alterations in cerebellar but not basal ganglia white matter tracts, leading them to speculate that these brain regions may play different roles in the development of repetitive behavior over time. The basal ganglia and cerebellum are tightly interconnected, both functionally and structurally, and correspondingly their influence on the development of motor and other behaviors are thought to be intertwined [102]. Thus, the older children in this study may represent a later developmental stage in which repetitive behaviors are more dependent on basal ganglia rather than cerebellar white matter.

Altered FA (or FA_T) is often considered an indicator of structural connectivity, reflecting factors such as aberrant myelination, but may also correspond to differences in other micro-structural properties (e.g., microtubule density). FW is thought to capture partial volume effects from extracellular space, as the diffusion-weighting time in common imaging sequences is such that FW signal most likely originates from spaces larger than a few tens of microns [103]. In the context of the results from this study, increased FW in ASD may reflect microstructural properties such as reduced density of glial cells in these white matter tracts [104] or neuroinflammation [19]. In support of findings from the present study, research using neurite orientation and dispersion imaging (NODDI) identified higher isotropic volume fraction in white matter of individuals with ASD, which was similarly interpreted as increased extracellular free-water [105]. Brain development in ASD is thought to be affected by “over-pruning” and increased FW could also reflect this process [106]. In conditions such as Parkinson’s disease, FW is also thought to reflect atrophic neurodegeneration [13–16], but we do not suspect neurodegeneration to be driving the present findings from children and adolescents with ASD.

Limitations

This study was performed on a deidentified dataset from the NDA, and thus we did not control data collection methods. In our data analysis we covaried for scanner type to account for small differences in imaging acquisition parameters, but information regarding the testing site from which each participant’s data originated was unavailable. Thus, this study cannot account for potential variability due to testing site. The white matter pathways

evaluated in this study were chosen due to their hypothesized relevance to RRB. Differences between ASD and TD individuals that may occur outside basal ganglia and cerebellar pathways, and their potential relationship to RRB, were not examined. The diffusion MRI data analyzed in this retrospective study were acquired with a single diffusion-weighted shell ($b=1000$ s/mm²). It has been demonstrated that when applying a two-compartment model to single-shell diffusion MRI data, changes in FW may be difficult to disentangle from tissue mean-diffusivity changes, and that multi-shell diffusion data offers improved FW estimates compared to single-shell data [107]. However, when only single-shell data are available, as was the case for this dataset, recent work has shown that applying a two-compartment model (i.e., free-water) provides increased signal-to-noise ratio and greater sensitivity than fitting a single compartment model to single shell data [108]. Although FA_T and FW capture aspects of tissue microstructure, the analyses performed here cannot determine the specific microstructural underpinnings of those differences; post-mortem experiments in clinical populations or work in animal models may elucidate how these metrics correspond to microstructural alterations in ASD. Lastly, although mean IQ score in the ASD group was significantly lower than mean IQ of the TD group, individuals in the ASD group had IQ in the normal range. We did not covary for IQ in this study, because it has been suggested that IQ is inappropriate to include as a covariate in studies of neurodevelopmental disorders, as differences in IQ are often part of the phenomena of the condition being studied [109]. It is unknown whether the findings from this study extend to individuals with ASD that have lower IQ scores.

Conclusions

In this study we used neuroimaging data available from the NDA to assess gray matter volume and white matter microstructure of the basal ganglia and cerebellum in ASD. These novel findings demonstrate that cortico-basal ganglia white matter microstructure is altered in ASD and linked to RRB. FW in cortico-basal ganglia and intra-basal ganglia white matter was more sensitive to group differences in ASD, whereas cortico-basal ganglia FA_T was more closely linked to RRB. In contrast, we found no significant difference for basal ganglia or cerebellar gray matter volumes in ASD. Sex-related differences in brain volume and microstructure were present in both ASD and TD groups and did not interact with diagnosis. Prior diffusion imaging investigations of white matter in ASD may have been impacted by partial volume effects of extracellular free-water, especially in basal ganglia pathways proximal to the ventricles. Future diffusion imaging investigations in ASD may benefit from quantification of

FW and corresponding correction of FA to account for partial volume effects in order to better understand how basal ganglia white matter is affected in ASD, and how such measures are associated with expression or attenuation of RRB.

Abbreviations

ASD	Autism spectrum disorder
RRB	Restricted, repetitive behavior
MRI	Magnetic resonance imaging
DTI	Diffusion tensor imaging
TD	Typically developing
NDA	National Institute of Mental Health Data Archive
ROI(s)	Region(s) of interest
IQ	Intelligence quotient
FOV	Field of view
TR	Repetition time
TE	Echo time
ANCOVA	Analysis of covariance
ADI-R	Autism Diagnostic Interview-Revised
RBS-R	Repetitive Behavior Scale-Revised
SCQ	Social Communication Questionnaire
ANTs	Advanced Normalization Tools
BET	Brain Extraction Tool
FDR	False discover rate
FSL	FMRIB Software Library
FA	Fractional anisotropy
FA _T	Free-water corrected fractional anisotropy
FW	Free-water
DLPFC	Dorsolateral prefrontal cortex
M1-U	Primary motor cortex, upper-extremity
MFG	Middle frontal gyrus
SN	Substantia nigra
SNpc	Substantia nigra pars compacta
SNpr	Substantia nigra pars reticulata
GPe	Globus pallidus externa
STN	Subthalamic nucleus
SCP	Superior cerebellar peduncle

Supplementary Information

The online version contains supplementary material available at <https://doi.org/10.1186/s13229-023-00581-2>.

Additional file 1: Supplementary materials (Tables S1–S5).

Acknowledgements

Data and/or research tools used in the preparation of this manuscript were obtained from the NIH-supported National Institute of Mental Health Data Archive (NDA). NDA is a collaborative informatics system created by the National Institutes of Health to provide a national resource to support the sharing of federally-funded data for accelerating research. Dataset identifier(s): collection ID #2021, study-specific dataset ID #1823 (<http://dx.doi.org/https://doi.org/10.15154/1528130>). This manuscript reflects the views of the authors and may not reflect the opinions or views of the NIH or of the Submitters submitting original data to NDA.

Author contributions

BW identified and accessed data from the NDA, performed data processing and analysis, and wrote the manuscript. DA developed white matter tract templates, performed data processing, and contributed to the manuscript. AF assisted with data analysis, interpretation of findings, and provided major contributions to the manuscript. CB and HK assisted with data organization and data pre-processing. DV helped with study design, provided computational resources for data analysis, and provided major contributions to the manuscript. ML helped with study conceptualization and design, interpretation of findings, and provided major contributions to the manuscript.

Funding

This work was supported by the University of Florida Clinical and Translational Science Institute [Non-Patient Oriented Pilot Project Award] and the American Psychological Association [Dissertation Research Award].

Availability of data and materials

The dataset supporting the conclusions of this article is available in the National Institute of Mental Health Data Archive (NDA): collection ID #2021.

Declarations

Ethics approval and consent to participate

This study was performed on a deidentified dataset from the NIH-supported National Institute of Mental Health Data Archive (NDA). The institutional review board at the University of Florida approved all procedures surrounding the access, storage, and use of these data.

Consent for publication

Not applicable.

Competing interests

None of the authors have potential competing interest to be disclosed.

Author details

¹Department of Applied Physiology and Kinesiology, University of Florida, P.O. Box 118205, Gainesville, FL 32611, USA. ²Vanderbilt Memory and Alzheimer's Center, Department of Neurology, Vanderbilt School of Medicine, Nashville, TN, USA. ³Department of Neurology, Vanderbilt Genetics Institute, Vanderbilt School of Medicine, Nashville, TN, USA. ⁴Department of Psychology, University of Florida, Gainesville, FL, USA. ⁵Department of Psychiatry, University of Florida, Gainesville, FL, USA. ⁶Department of Pharmacology, College of Medicine, University of Arizona, Tucson, AZ, USA. ⁷Department of Biomedical Engineering, University of Florida, Gainesville, FL, USA. ⁸Department of Neurology, Fixel Center for Neurological Diseases, Program in Movement Disorders and Neurorestoration, University of Florida, Gainesville, FL, USA.

Received: 18 August 2023 Accepted: 23 December 2023

Published online: 23 January 2024

References

- Boyd BA, McDonough SG, Bodfish JW. Evidence-based behavioral interventions for repetitive behaviors in autism. *J Autism Dev Disord*. 2012;42:1236–48.
- Rapp JT, Vollmer TR. Stereotypy I: a review of behavioral assessment and treatment. *Res Dev Disabil*. 2005;26:527–47.
- Rapp JT, Vollmer TR. Stereotypy II: a review of neurobiological interpretations and suggestions for an integration with behavioral methods. *Res Dev Disabil*. 2005;26:548–64.
- Carrasco M, Volkmar FR, Bloch MH. Pharmacologic treatment of repetitive behaviors in autism spectrum disorders: evidence of publication bias. *Pediatrics*. 2012;129:e1301–1310.
- King BH, et al. Baseline factors predicting placebo response to treatment in children and adolescents with autism spectrum disorders: a multisite randomized clinical trial. *JAMA Pediatr*. 2013;167:1045–52.
- Mahajan R, Mostofsky SH. Neuroimaging endophenotypes in autism spectrum disorder. *CNS Spectr*. 2015;20:412–26.
- Mash LE, Reiter MA, Linke AC, Townsend J, Müller R-A. Multimodal approaches to functional connectivity in autism spectrum disorders: an integrative perspective. *Dev Neurobiol*. 2018;78:456–73.
- Müller R-A, et al. Underconnected, but how? A survey of functional connectivity MRI studies in autism spectrum disorders. *Cereb Cortex*. 2011;21:2233–43.
- Rane P, et al. Connectivity in autism: a review of MRI connectivity studies. *Harv Rev Psychiatry*. 2015;23:223–44.
- Travers BG, et al. Diffusion tensor imaging in autism spectrum disorder: a review. *Autism Res*. 2012;5:289–313.

11. Ameis SH, Catani M. Altered white matter connectivity as a neural substrate for social impairment in Autism Spectrum Disorder. *Cortex*. 2015;62:158–81.
12. Wilkes BJ, Lewis MH. The neural circuitry of restricted repetitive behavior: magnetic resonance imaging in neurodevelopmental disorders and animal models. *Neurosci Biobehav Rev*. 2018;92:152–71.
13. Pasternak O, Sochen N, Gur Y, Intrator N, Assaf Y. Free water elimination and mapping from diffusion MRI. *Magn Reson Med*. 2009;62:717–30.
14. Yang Y, et al. White matter microstructural metrics are sensitively associated with clinical staging in Alzheimer's disease. *Alzheimers Dement (Amst)*. 2023;15:e12425.
15. Ofori E, et al. Increased free water in the substantia nigra of Parkinson's disease: a single-site and multi-site study. *Neurobiol Aging*. 2015;36:1097–104.
16. Ofori E, et al. Longitudinal changes in free-water within the substantia nigra of Parkinson's disease. *Brain*. 2015;138:2322–31.
17. Ofori E, et al. Free water improves detection of changes in the substantia nigra in parkinsonism: a multisite study. *Mov Disord*. 2017;32:1457–64.
18. Planetta PJ, et al. Free-water imaging in Parkinson's disease and atypical parkinsonism. *Brain*. 2016;139:495–508.
19. Febo M, et al. Diffusion magnetic resonance imaging-derived free water detects neurodegenerative pattern induced by interferon- γ . *Brain Struct Funct*. 2020;225:427–39.
20. Surgent O, et al. Brainstem white matter microstructure is associated with hyporesponsiveness and overall sensory features in autistic children. *Mol Autism*. 2022;13:48.
21. Walsh MJM, et al. Preliminary findings of accelerated visual memory decline and baseline brain correlates in middle-age and older adults with autism: the case for hippocampal free-water. *Front Aging Neurosci*. 2022;14:1029166.
22. Fatemi SH, et al. Consensus paper: pathological role of the cerebellum in autism. *Cerebellum*. 2012;11:777–807.
23. Stoodley CJ, et al. Altered cerebellar connectivity in autism and cerebellar-mediated rescue of autism-related behaviors in mice. *Nat Neurosci*. 2017;20:1744–51.
24. Subramanian K, et al. Basal ganglia and autism—a translational perspective. *Autism Res*. 2017;10:1751–75.
25. Maenner MJ, et al. Prevalence and characteristics of autism spectrum disorder among children aged 8 years—autism and developmental disabilities monitoring network, 11 Sites, United States, 2020. *MMWR Surveill Summ*. 2023;72:1–14.
26. Floris DL, et al. Towards robust and replicable sex differences in the intrinsic brain function of autism. *Mol Autism*. 2021;12:19.
27. Floris DL, et al. The link between autism and sex-related neuroanatomy, and associated cognition and gene expression. *Am J Psychiatry*. 2023;180:50–64.
28. Irimia A, Torgerson CM, Jacokes ZJ, Van Horn JD. The connectomes of males and females with autism spectrum disorder have significantly different white matter connectivity densities. *Sci Rep*. 2017;7:46401.
29. Irimia A, et al. Support vector machines, multidimensional scaling and magnetic resonance imaging reveal structural brain abnormalities associated with the interaction between autism spectrum disorder and sex. *Front Comput Neurosci*. 2018;12:93.
30. Zhang W, et al. Revisiting subcortical brain volume correlates of autism in the ABIDE dataset: effects of age and sex. *Psychol Med*. 2018;48:654–68.
31. Walsh MJM, Wallace GL, Gallegos SM, Braden BB. Brain-based sex differences in autism spectrum disorder across the lifespan: a systematic review of structural MRI, fMRI, and DTI findings. *Neuroimage Clin*. 2021;31: 102719.
32. Van Wijngaarden-Cremers PJM, et al. Gender and age differences in the core triad of impairments in autism spectrum disorders: a systematic review and meta-analysis. *J Autism Dev Disord*. 2014;44:627–35.
33. Siracusano M, et al. Sex differences in autism spectrum disorder: repetitive behaviors and adaptive functioning. *Children (Basel)*. 2021;8:325.
34. Antezana L, et al. Gender differences in restricted and repetitive behaviors and interests in youth with autism. *Autism Res*. 2018. <https://doi.org/10.1002/aur.2049>.
35. Knutsen J, Crossman M, Perrin J, Shui A, Kuhlthau K. Sex differences in restricted repetitive behaviors and interests in children with autism spectrum disorder: an autism treatment network study. *Autism*. 2018. <https://doi.org/10.1177/1362361318786490>.
36. Frazier TW, Georgiades S, Bishop SL, Hardan AY. Behavioral and cognitive characteristics of females and males with autism in the Simons Simplex Collection. *J Am Acad Child Adolesc Psychiatry*. 2014;53(329–340):e1–3.
37. Bodfish JW, Symons FJ, Parker DE, Lewis MH. Varieties of repetitive behavior in autism: comparisons to mental retardation. *J Autism Dev Disord*. 2000;30:237–43.
38. Berument SK, Rutter M, Lord C, Pickles A, Bailey A. Autism screening questionnaire: diagnostic validity. *Br J Psychiatry*. 1999;175:444–51.
39. Keuken MC, Forstmann BU. A probabilistic atlas of the basal ganglia using 7 T MRI. *Data Brief*. 2015;4:577–82.
40. Tziortzi AC, et al. Imaging dopamine receptors in humans with [11C]-(+)-PHNO: dissection of D3 signal and anatomy. *Neuroimage*. 2011;54:264–77.
41. Diedrichsen J, Balsters JH, Flavell J, Cussans E, Ramnani N. A probabilistic MR atlas of the human cerebellum. *Neuroimage*. 2009;46:39–46.
42. Diedrichsen J, et al. Imaging the deep cerebellar nuclei: a probabilistic atlas and normalization procedure. *Neuroimage*. 2011;54:1786–94.
43. Avants BB, et al. The optimal template effect in hippocampus studies of diseased populations. *Neuroimage*. 2010;49:2457–66.
44. Benjamini Y, Hochberg Y. Controlling the false discovery rate: a practical and powerful approach to multiple testing. *J R Stat Soc Ser B Methodol*. 1995;57:289–300.
45. Burciu RG, et al. Progression marker of Parkinson's disease: a 4-year multi-site imaging study. *Brain*. 2017;140:2183–92.
46. Mitchell T, et al. Neurite orientation dispersion and density imaging (NODDI) and free-water imaging in Parkinsonism. *Hum Brain Mapp*. 2019. <https://doi.org/10.1002/hbm.24760>.
47. Mitchell T, et al. Advanced diffusion imaging to track progression in Parkinson's disease, multiple system atrophy, and progressive supranuclear palsy. *Neuroimage Clin*. 2022;34: 103022.
48. Archer DB, et al. Development and validation of the automated imaging differentiation in parkinsonism (AID-P): a multi-site machine learning study. *Lancet Digit Health*. 2019;1:e222–31.
49. Wilkes BJ, et al. Distinct cortical and subcortical predictors of Purdue Pegboard decline in Parkinson's disease and atypical parkinsonism. *NPJ Parkinsons Dis*. 2023;9:85.
50. Archer DB, Vaillancourt DE, Coombes SA. A template and probabilistic atlas of the human sensorimotor tracts using diffusion MRI. *Cereb Cortex*. 2018;28:1685–99.
51. Archer DB, Coombes SA, McFarland NR, DeKosky ST, Vaillancourt DE. Development of a transcallosal tractography template and its application to dementia. *Neuroimage*. 2019;200:302–12.
52. Sotiropoulos SN, et al. Advances in diffusion MRI acquisition and processing in the Human Connectome Project. *Neuroimage*. 2013;80:125–43.
53. Mayka MA, Corcos DM, Leurgans SE, Vaillancourt DE. Three-dimensional locations and boundaries of motor and premotor cortices as defined by functional brain imaging: a meta-analysis. *Neuroimage*. 2006;31:1453–74.
54. Prodoehl J, Yu H, Little DM, Abraham I, Vaillancourt DE. Region of interest template for the human basal ganglia: comparing EPI and standardized space approaches. *Neuroimage*. 2008;39:956–65.
55. Hanaie R, et al. Altered microstructural connectivity of the superior cerebellar peduncle is related to motor dysfunction in children with autistic spectrum disorders. *Cerebellum*. 2013;12:645–56.
56. Estes A, et al. Basal ganglia morphometry and repetitive behavior in young children with autism spectrum disorder. *Autism Res*. 2011;4:212–20.
57. Hollander E, et al. Striatal volume on magnetic resonance imaging and repetitive behaviors in autism. *Biol Psychiatry*. 2005;58:226–32.
58. Rojas DC, et al. Regional gray matter volumetric changes in autism associated with social and repetitive behavior symptoms. *BMC Psychiatry*. 2006;6:56.
59. Sears LL, et al. An MRI study of the basal ganglia in autism. *Prog Neuropsychopharmacol Biol Psychiatry*. 1999;23:613–24.
60. Qiu T, et al. Two years changes in the development of caudate nucleus are involved in restricted repetitive behaviors in 2-5-year-old children with autism spectrum disorder. *Dev Cogn Neurosci*. 2016;19:137–43.

61. Langen M, et al. Changes in the development of striatum are involved in repetitive behavior in autism. *Biol Psychiatry*. 2014;76:405–11.
62. Eisenberg IW, Wallace GL, Kenworthy L, Gotts SJ, Martin A. Insistence on sameness relates to increased covariance of gray matter structure in autism spectrum disorder. *Mol Autism*. 2015;6:54.
63. Abbott AE, et al. Repetitive behaviors in autism are linked to imbalance of corticostriatal connectivity: a functional connectivity MRI study. *Soc Cogn Affect Neurosci*. 2018;13:32–42.
64. Delmonte S, Gallagher L, O'Hanlon E, McGrath J, Balsters JH. Functional and structural connectivity of frontostriatal circuitry in Autism Spectrum Disorder. *Front Hum Neurosci*. 2013;7:430.
65. Di Martino A, et al. Aberrant striatal functional connectivity in children with autism. *Biol Psychiatry*. 2011;69:847–56.
66. Langen M, et al. Fronto-striatal circuitry and inhibitory control in autism: findings from diffusion tensor imaging tractography. *Cortex*. 2012;48:183–93.
67. Uddin LQ, et al. Salience network-based classification and prediction of symptom severity in children with autism. *JAMA Psychiat*. 2013;70:869–79.
68. McKinnon CJ, et al. Restricted and repetitive behavior and brain functional connectivity in infants at risk for developing autism spectrum disorder. *Biol Psychiatry Cogn Neuroimaging*. 2019;4:50–61.
69. Bertelsen N, et al. Imbalanced social-communicative and restricted repetitive behavior subtypes of autism spectrum disorder exhibit different neural circuitry. *Commun Biol*. 2021;4:574.
70. Ilioska I, et al. Connectome-wide mega-analysis reveals robust patterns of atypical functional connectivity in autism. *Biol Psychiatry*. 2023;94:29–39.
71. Akkermans SEA, et al. Fronto-striatal functional connectivity correlates with repetitive behaviour across autism spectrum disorder and obsessive-compulsive disorder. *Psychol Med*. 2019;49:2247–55.
72. Peterson BS, et al. Using tissue microstructure and multimodal MRI to parse the phenotypic heterogeneity and cellular basis of autism spectrum disorder. *J Child Psychol Psychiatry*. 2022;63:855–70.
73. Cheung C, et al. White matter fractional anisotropy differences and correlates of diagnostic symptoms in autism. *J Child Psychol Psychiatry*. 2009;50:1102–12.
74. Hau J, et al. Supplementary and premotor aspects of the corticospinal tract show links with restricted and repetitive behaviors in middle-aged adults with autism spectrum disorder. *Cereb Cortex*. 2021;31:3962–72.
75. Kirkovski M, Enticott PG, Maller JJ, Rossell SL, Fitzgerald PB. Diffusion tensor imaging reveals no white matter impairments among adults with autism spectrum disorder. *Psychiatry Res*. 2015;233:64–72.
76. Nordahl CW, et al. Sex differences in the corpus callosum in preschool-aged children with autism spectrum disorder. *Mol Autism*. 2015;6:26.
77. Turner AH, Greenspan KS, van Erp TGM. Pallidum and lateral ventricle volume enlargement in autism spectrum disorder. *Psychiatry Res Neuroimaging*. 2016;252:40–5.
78. Badre D, D'Esposito M. Is the rostro-caudal axis of the frontal lobe hierarchical? *Nat Rev Neurosci*. 2009;10:659–69.
79. Barbas H, Pandya DN. Architecture and intrinsic connections of the prefrontal cortex in the rhesus monkey. *J Comp Neurol*. 1989;286:353–75.
80. Yeterian EH, Pandya DN, Tomaiuolo F, Petrides M. The cortical connectivity of the prefrontal cortex in the monkey brain. *Cortex*. 2012;48:58–81.
81. Leh SE, Ptito A, Chakravarty MM, Strafella AP. Fronto-striatal connections in the human brain: a probabilistic diffusion tractography study. *Neurosci Lett*. 2007;419:113–8.
82. Zandbelt BB, Vink M. On the role of the striatum in response inhibition. *PLoS ONE*. 2010;5: e13848.
83. Shang CY, Wu YH, Gau SS, Tseng WY. Disturbed microstructural integrity of the frontostriatal fiber pathways and executive dysfunction in children with attention deficit hyperactivity disorder. *Psychol Med*. 2013;43:1093–107.
84. Koch K, Reess TJ, Rus OG, Zimmer C, Zaudig M. Diffusion tensor imaging (DTI) studies in patients with obsessive-compulsive disorder (OCD): a review. *J Psychiatr Res*. 2014;54:26–35.
85. McBride SD, Parker MO. The disrupted basal ganglia and behavioural control: an integrative cross-domain perspective of spontaneous stereotypy. *Behav Brain Res*. 2015;276:45–58.
86. Presti MF, Lewis MH. Striatal opioid peptide content in an animal model of spontaneous stereotypic behavior. *Behav Brain Res*. 2005;157:363–8.
87. Tanimura Y, King MA, Williams DK, Lewis MH. Development of repetitive behavior in a mouse model: roles of indirect and striosomal basal ganglia pathways. *Int J Dev Neurosci*. 2011;29:461–7.
88. Tanimura Y, Vaziri S, Lewis MH. Indirect basal ganglia pathway mediation of repetitive behavior: attenuation by adenosine receptor agonists. *Behav Brain Res*. 2010;210:116–22.
89. Baup N, et al. High-frequency stimulation of the anterior subthalamic nucleus reduces stereotyped behaviors in primates. *J Neurosci*. 2008;28:8785–8.
90. Becharod AR, Cacodcar N, King MA, Lewis MH. How does environmental enrichment reduce repetitive motor behaviors? Neuronal activation and dendritic morphology in the indirect basal ganglia pathway of a mouse model. *Behav Brain Res*. 2016;299:122–31.
91. Lewis MH, Rajpal H, Muehlmann AM. Reduction of repetitive behavior by co-administration of adenosine receptor agonists in C58 mice. *Pharmacol Biochem Behav*. 2019;181:110–6.
92. Wilkes BJ, Bass C, Korah H, Febo M, Lewis MH. Volumetric magnetic resonance and diffusion tensor imaging of C58/J mice: neural correlates of repetitive behavior. *Brain Imaging Behav*. 2019. <https://doi.org/10.1007/s11682-019-00158-9>.
93. Muehlmann AM, Maletz S, King MA, Lewis MH. Pharmacological targeting of striatal indirect pathway neurons improves subthalamic nucleus dysfunction and reduces repetitive behaviors in C58 mice. *Behav Brain Res*. 2020;391: 112708.
94. Pavál D. A dopamine hypothesis of autism spectrum disorder. *Dev Neurosci*. 2017;39:355–60.
95. Calabresi P, Picconi B, Tozzi A, Ghiglieri V, Di Filippo M. Direct and indirect pathways of basal ganglia: a critical reappraisal. *Nat Neurosci*. 2014;17:1022–30.
96. Hollander E, Wang AT, Braun A, Marsh L. Neurological considerations: autism and Parkinson's disease. *Psychiatry Res*. 2009;170:43–51.
97. Simmonds DJ, Hallquist MN, Asato M, Luna B. Developmental stages and sex differences of white matter and behavioral development through adolescence: a longitudinal diffusion tensor imaging (DTI) study. *Neuroimage*. 2014;92:356–68.
98. Beacher FD, et al. Autism attenuates sex differences in brain structure: a combined voxel-based morphometry and diffusion tensor imaging study. *AJNR Am J Neuroradiol*. 2012;33:83–9.
99. Retico A, et al. The effect of gender on the neuroanatomy of children with autism spectrum disorders: a support vector machine case-control study. *Mol Autism*. 2016;7:5.
100. Andrews DS, et al. A longitudinal study of white matter development in relation to changes in autism severity across early childhood. *Biol Psychiatry*. 2021;89:424–32.
101. Wolff JJ, et al. Neural circuitry at age 6 months associated with later repetitive behavior and sensory responsiveness in autism. *Mol Autism*. 2017;8:8.
102. Bostan AC, Strick PL. The basal ganglia and the cerebellum: nodes in an integrated network. *Nat Rev Neurosci*. 2018;19:338–50.
103. Pasternak O, Shenton ME, Westin C-F. Estimation of extracellular volume from regularized multi-shell diffusion MRI. *Med Image Comput Comput Assist Interv*. 2012;15:305–12.
104. Pasternak O, et al. Hockey Concussion Education Project, Part 2. Microstructural white matter alterations in acutely concussed ice hockey players: a longitudinal free-water MRI study. *J Neurosurg*. 2014;120:873–81.
105. Andica C, et al. Neurite orientation dispersion and density imaging reveals white matter microstructural alterations in adults with autism. *Mol Autism*. 2021;12:48.
106. Thomas MSC, Davis R, Karmiloff-Smith A, Knowland VCP, Charman T. The over-pruning hypothesis of autism. *Dev Sci*. 2016;19:284–305.
107. Golub M, Neto Henriques R, Gouveia Nunes R. Free-water DTI estimates from single b-value data might seem plausible but must be interpreted with care. *Magn Reson Med*. 2021;85:2537–51.
108. Chad JA, Sochen N, Chen JJ, Pasternak O. Implications of fitting a two-compartment model in single-shell diffusion MRI. *Phys Med Biol*. 2023;68:215012.
109. Dennis M, et al. Why IQ is not a covariate in cognitive studies of neurodevelopmental disorders. *J Int Neuropsychol Soc*. 2009;15:331–43.

Publisher's Note

Springer Nature remains neutral with regard to jurisdictional claims in published maps and institutional affiliations.